ULTRASONIC IMAGING 7, 252-263 (1985)

QUANTITATIVE TESTS OF A THREE-DIMENSIONAL GRAY SCALE TEXTURE MODEL

J. A. Zagzebski[1], E. L. Madsen[1], and M. M. Goodsitt[2]

[1]Department of Medical Physics
University of Wisconsin
Madison, WI 53706

[2] Department of Radiological Sciences
Massachusetts General Hospital
Boston, MA 02114

A three-dimensional model for gray scale texture in ultrasound B-mode images has been extended to enable absolute quantitative predictions of echo signal levels and texture characteristics. The quantitative aspects of the model are tested with a phantom in which the ultrasonic scattering properties as well as the ultrasonic attenuation coefficient and the speed of sound are known as functions of frequency. Good agreement between theoretical predictions and experimental results was found in the overall brightness of B-mode images, in pixel value histograms, and in an autocorrelation function analysis of images. Passing quantitative tests is additional evidence that the model is a reliable tool for computer simulations involving many important facets of ultrasound B-mode imaging and tissue characterization.

Key words: B-mode imaging; image texture; image speckle; lesion detection; mathematical models; quantitative imaging; tissue phantoms.

1. INTRODUCTION

In a previous paper [1], we described a three-dimensional model for production of gray scale texture on ultrasound B-mode images. One aspect of the model provides for computation of time dependent echo signal waveforms for the case in which an ultrasound transducer is placed in contact with an attenuating medium containing a spatially random distribution of scatterers. A gray scale image is produced by computing echo signals for simulated, successive linear translations of the transducer and then modeling the signal processing and echo signal detection process occurring in ultrasound B-mode scanners. The model allows for incorporation of closely simulated instrumental factors, including the frequency characteristics of any transducer-pulser-receiver combinations used in forming images. The model was tested by comparing computed images with experimental images obtained using a graphite-in-gelatin tissue-mimicking phantom in which the physical properties of the scatterers, such as shape, diameter distribution and concentration, were not specified or well known. The broad range of scatterer diameters existing in the phantom was approximated with a single scatterer diameter which was representative of that range. The overall brightness of the experimental and theoretical images were made to agree by choice of a constant. Computed images agree with experimental images semiquantitatively in terms of the overall texture appearance, the variation in texture with distance from the transducer, as well as the effects of varying the transducer center frequency and other signal processing parameters.

0161-7346/85 $3.00

Thus, two shortcomings of the experimental verification of the texture model have been that relative rather than absolute signal levels were compared and that scatterer characteristics were not accurately represented. In the present work, these restrictions have been removed by constructing and modeling a phantom in which the scatterers are well characterized in terms of their concentration, diameter distribution, and relevant physical properties; theory is compared with experiment in an absolute quantitative fashion by incorporating into the model the above information about the scatterers including computed scattering functions and excluding adjustable constants.

The texture model provides insight into the nature of gray-scale texture patterns on ultrasound images; however, its main purpose is to enable computer simulations of ultrasound B-mode images for a variety of imaging situations and different scanning and signal processing parameters. The model is three-dimensional, yet computationally efficient. This allows detailed studies of factors related to "fill-in" of echo-free regions and detectability of simulated lesions having various scattering levels, sizes, and positions in the imaged "slice."

2. OUTLINE OF THE THREE-DIMENSIONAL TEXTURE MODEL

The three-dimensional model has been described in detail in a previous report [1] and is reviewed briefly here. The present analysis differs from that in our earlier report in that the ultrasonic scattering properties of the medium are retained, and echo signal voltages from a phantom are computed absolutely. The notation employed in the present paper is that found in [2].

Several assumptions are made in the model in order to compute echo signal waveforms and gray scale images. The transducers that are included have active elements in the shape of spherical shell sections with circular boundaries. The active (radiating) element of each transducer consists of a uniform distribution of identical point sources vibrating in unison. The transducer is placed in contact with a tissue-mimicking phantom, whose speed of sound and attenuation properties over the diagnostic frequency range are known. The same transducer detects echo signals arising from scatterers in the medium. These scatterers are assumed to be identical and spatially randomly distributed.

Let $p(\vec{r},t)$ represent the time-dependent incident pressure pulse at field point $\vec{r}$ produced by the transducer. This quantity is represented as a superposition of a complete set of continuous wave beams varying sinusoidally in time [1,2]. It is shown in [2] that, since $p(\vec{r},t)$ is real, the superposition can be written:

$$p(\vec{r},t) = \int_{-\infty}^{\infty} d\omega B_o(\omega) A_o(\vec{r},\omega) e^{-i\omega t} \tag{1}$$

where t is the time, ω is the angular frequency and $B_o(\omega)$ is a complex superposition coefficient. $A_o(\vec{r},\omega)$ is proportional to the Rayleigh integral [3] (for the case in which the normal component of the velocity at any instant of time is the same at all points on the radiating surface) integrated over the active area of the transducer. Specifically,

$$A_o(\vec{r},\omega) = \int_S \frac{e^{ik[\vec{r}-\vec{r}']}}{[\vec{r}-\vec{r}']} ds', \tag{2}$$

where $k = \frac{\omega}{c(\omega)} + i\alpha(\omega)$ is the complex wave number, $c(\omega)$ is the speed of sound in the medium at frequency ω, and $\alpha(\omega)$ is the attenuation coefficient in the medium at frequency ω. S represents the surface of the transducer, ds' is an area element on the transducer surface and $\vec{r}'$ is the position vector of the area element ds'.

The medium is assumed to contain a spatially-random distribution of small scatterers. If a scatterer is positioned at $\vec{r}$ we can approximate the incident wave packet on the scatterer as a superposition of plane waves such that a single plane wave correponds to the components of the pressure wave at frequencies between ω and $\omega + d\omega$. The component of the scattered pressure wave at position $\vec{r}''$ due to a scatterer at $\vec{r}$, for frequencies between ω and $\omega + d\omega$, is given by

$$dp_s(\vec{r},\vec{r}'',\omega,t) = d\omega\, B_o(\omega)A_o(\vec{r},\omega)e^{-i\omega t}\, \Phi(k,\cos\theta)\, \frac{e^{ik[\vec{r}-\vec{r}'']}}{[\vec{r}-\vec{r}'']}, \tag{3}$$

where $\Phi(k,\cos\theta)$ is the angle distribution function [4] for the particle in the direction θ for wave number k.

The scattered wave will exert a force on the transducer, which may be found by integrating the expression in Eq. (3) over S, the face of the transducer:

$$dF_s(\vec{r},\omega,t) = d\omega B_o(\omega)A_o(\vec{r},\omega)e^{-i\omega t}\, \Phi(k,\cos\theta) \int_S \frac{e^{ik[\vec{r}-\vec{r}'']}}{[\vec{r}-\vec{r}'']}\, ds'' \tag{4}$$

where $\vec{r}''$ is the position vector of the area element ds" on the transducer surface. However, since

$$\int_S \frac{e^{ik[\vec{r}-\vec{r}']}}{[\vec{r}-\vec{r}']}\, ds' = \int_S \frac{e^{ik[\vec{r}-\vec{r}'']}}{[\vec{r}-\vec{r}'']}\, ds'' \tag{5}$$

$$dF_s(\vec{r},\omega,t) = d\omega B_o(\omega)[A_o(\vec{r},\omega)]^2\, e^{-i\omega t}\, \Phi(k,\cos\theta)\ . \tag{6}$$

If the scatterer is far enough from the transducer or if the scatterer is monopolar in nature, $\Phi(k,\cos\theta)$ can be approximated by $\Phi(k,-1) = \Phi(k)$.

For situations considered here many scatterers are distributed throughout the medium. The total force at time t is:

$$F_s(t) = \int_{-\infty}^{\infty} d\omega B_o(\omega)e^{-i\omega t} \sum_{i=1}^{Q} [A_o(\vec{r}_i,\omega)]^2\, \Phi_i(k). \tag{7}$$

The sum over i includes all scatterers in the field. The time, t, determines which scatterers contribute, however.

Let $T(\omega)$ be a complex receiver transfer function for the transducer amplifier system. The echo signal voltage at time t due to all scatterers is given by

$$s(t) = \int_{-\infty}^{\infty} d\omega\ T(\omega)B_o(\omega)\ e^{-i\omega t} \sum_{i=1}^{Q} [A_o(\vec{r}_i,\omega)]^2\, \Phi_i(k). \tag{8}$$

As Eq. (8) suggests, computing the echo signal voltage requires the solution of a double integral over the surface of the transducer for each scatterer in the medium. Computational efficiency is brought about by exploiting the axial symmetry of the problem when circular transducers are used. A single integral expression [5] is used to solve for the pressure field of the transducer. This calculation is done for each field point of interest for frequencies throughout the bandpass of the transducer. The adequacy of the algorithm and model for the transducer field has been verified both for continuous wave and pulsed excitation [5,6].

Axial symmetry can also be exploited when computing echo signals from scatterers in the medium [1,7]. Each scatterer lying within a small annular ring of thickness Δz and width ΔR will be bathed with about the same incident pressure. (See figure 3 of Reference [1].) If the scatterers are identical, each will contribute identically to the force on the transducer face. In our model the imaged field is divided into sets of annular rings. The contribution to s(t) from all scatterers in a given ring is equal to the contribution from a single scatterer multiplied by the number of scatterers in that ring.

Values for $A_o(\vec{r},\omega)$ are computed only for points on a circle centrally located within the ring volume element. Tests have demonstrated that for 2.25 MHz and 3.5 MHz pulsed transducers a scheme employing 25 rings at each of 197 depths, with ΔR = 0.4 mm and Δz = 0.1 mm, yielded convergent results [1]. These ring dimensions were employed in the present study.

To calculate the number of scatterers in each ring it is assumed that scatterers are spatially randomly distributed. The object being scanned is divided into rectangular volume elements called VOXELS. The dimensions of each VOXEL are 0.2 mm x 0.2 mm x 19.7 mm. A Poisson random number generator designates the number of scatterers in each voxel; then a uniform random number generator determines the axial position of each particle. The number of scatterers in each ring is computed using the voxel information. A voxel is considered to intersect a given ring (and scatterers in that voxel are added to the intersected ring) if the vertical line passing through the center of the voxel intersects that ring. In this study, the process was repeated for 50 transducer positions, with a 0.4 mm linear translation of the transducer assumed between positions.

3. EXPERIMENTAL PROCEDURES AND DATA ANALYSIS

3.1. Phantom for Quantitative Tests

Quantitative tests of the model were done using a soft tissue-like phantom in which the attenuation and speed of sound were determined experimentally and the ultrasonic scattering properties are well-known. The phantom is in the shape of a 6 cm x 12 cm x 15 cm rectangular parallelepiped with a 50 μ thick Saran Wrap (Dow Chemical, Midland, MI) window of area 6 cm x 12 cm. It was built using techniques described previously [8,9]. The tissue-mimicking material consists of gelatin laced with graphite powder. The concentration of powder was selected to produce the desired level of ultrasonic attenuation. In some phantoms the graphite powder also produces backscattered echo signals [1,8,9]. However, it is difficult to model quantitatively the scattering properties of such material because of the presence of a wide range of scatterer sizes and complex scatterer shapes. Therefore, in the present phantom a very fine-grained graphite powder was used to control the attenuation. This material produces negligible backscattering.

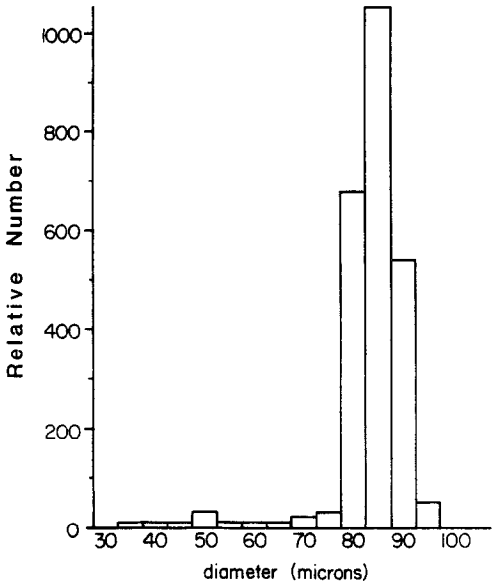

Fig. 1 Histogram illustrating the diameter distribution of glass bead scatterers in the quantitative texture phantom.

Scattered echo signals from within the phantom are due to the presence of microscopic glass beads (Potters Industries, Hasbrouck, NJ) distributed in random positions throughout the tissue-mimicking material. Glass beads were sieved to produce a mixture in which the mean diameter is 84 μm. The final diameter distribution was determined using a microscope [10] and is narrow, as shown in figure 1. The mean scatterer concentration in the phantom is $4.74/mm^3$.

At the time of manufacture of the phantom, an 8 cm diameter, 2.5 cm thick "test cylinder" was filled with the same molten gel-graphite powder-glass beads used in the bulk of the phantom. The speed of sound and the attenuation coefficient vs. frequency were measured for contents of the test cylinder using a narrow band substitution technique [8]. The results for the bulk material are shown in table I. A fit to the data on the attenuation coefficient is 0.45 $dB/cm\text{-}MHz^{1.06}$ x $f^{1.06}$, where f is the ultrasonic frequency in MHz. The speed of sound is 1546 m/s. These parameters were used in calculating the $A_o(\vec{r},\omega)$ values in Eq. (8).

Table I. Physical properties used to calculate the scatter function of the glass beads in the texture phantom

Longitudinal speed of sound	5572 m/s
Density	2.5×10^3 kg/m³
Poisson's ratio	0.21
Background speed of sound	1546 m/s
Background density	1.04×10^3 kg/m³

Table I also presents values for parameters used to calculate the scattering function, $\Phi(k)$. Physical properties supplied by the manufacturer were assumed to apply for the glass bead scatterers, and $\Phi(k)$ was evaluated using Eq. (31) of Faran [11]. Results for scattering in the 180^{o} direction (ie, backscattering) were used for each of the rings.

3.2. Recording Echo Signals From the Phantom

The apparatus used to record echo signals from the phantom and process experimental and theoretical signals to form image files has been described in detail previously [1]. Briefly, a focused ultrasonic transducer was placed in contact with the Saran layer window of the phantom and scanned in a linear fashion. The transducer was excited with a Panametrics 5052 pulser-receiver system. Amplified echo signals from the depth of interest were digitized at a 50 MHz rate in a Biomation 8100 Transient Recorder (Gould), interfaced to an LSI 11/23 computer (Digital Equipment Corporation), and then stored on disk. There was a 0.4 mm separation between successive transducer positions from which echo signals were recorded.

Two broadband transducers were employed in quantitative tests of the texture model. One has a 3.5 MHz nominal frequency, 19 mm diameter projected aperture, with an 11.0 cm radius of curvature; the other has a 2.25 MHz nominal frequency, 19 mm diameter aperture and a 14 cm radius of curvature.

3.3 Determining $T(\omega)B_{o}(\omega)$ For The Transducer-Pulser-Receiver

In our studies, the product of the superposition coefficient, $B_{o}(\omega)$, and the value of the transducer-receiver transfer function, $T(\omega)$, at each frequency ω, is determined using the echo signal from a small spherical reflector positioned at the radius of curvature of the transducer. A 0.35 mm diameter stainless steel ball bearing was suspended in a cylinder of clear gelatin as shown in figure 2. The ball bearing was positioned at the center of curvature of the transducer by using the pulse-echo delay time to position it at the appropriate axial distance and then applying small translations in directions perpendicular to the axis to find the spot where the peak echo signal occurred. Transmitter output and damping controls on the pulser receiver were identical to those used to record signals from the phantom. The amplifier gain was adjusted to utilize the full dynamic range of the transient recorder. Any difference between the receiver gain settings used for the ball bearing reference signal and those used to record echo signals from the phantom were taken into account in the data reduction.

The ball bearing, when used with Faran's theory [11], constitutes a quantitative reference scatterer allowing the complex quantity $T(\omega)B_{o}(\omega)$ to

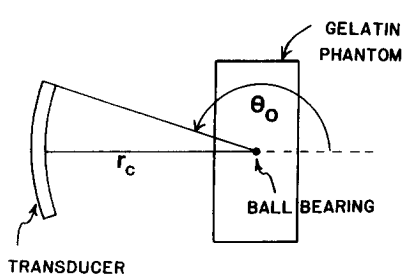

Fig. 2 Experimental method for determining $A_{o}(\omega)T(\omega)$ for the transducer-pulser-receiver system that was modeled. $A_{o}(\omega)T(\omega)$ was calculated using Eq. 12 in the text.

be determined at all relevant frequencies. For this situation, Eq. (4) becomes

$$dF_s(\vec{r},\omega,t) = d\omega B_o(\omega)A_o(r_c,\omega)\, e^{-i\omega t}\left[2\pi r_c^2 \int_{\pi}^{\theta_o} B_F(\omega,r_c,\theta)\sin\theta d\theta\right], \tag{9}$$

where $B_F(\omega,r_c,\theta)$ is calculated from the Faran theory and corresponds to the complex pressure scattered from the sphere at distance r_c and scattering angle θ. The quantity r_c is the radius of curvature of the transducer's radiating element and $\pi - \theta_o$ is the half angle subtended by the radiating element as seen from the center of curvature.

Introducing the receiving transfer function and integrating over all frequencies, the echo signal voltage at time t due to the spherical reference reflector is

$$s_{bb}(t) = \int_{-\infty}^{\infty} d\omega' T(\omega')\, B_o(\omega')A_o(r_c,\omega)e^{-i\omega' t}\left[2\pi r_c^2 \int_{\pi}^{\theta_o} B_F(\omega',r_c,\theta)\sin\theta d\theta\right] \tag{10}$$

where dummy variables for frequency have been primed. The Fourier transform of the echo voltage is

$$s_{bb}(\omega) = \frac{1}{2\pi}\int_{-\infty}^{\infty} dt\; s_{bb}(t)e^{i\omega t} \tag{11a}$$

$$= T(\omega)B_o(\omega)A_o(r_c,\omega)\left[2\pi r_c^2 \int_{\pi}^{\theta_o} B_F(\omega,r_c,\theta)\sin\theta d\theta\right]. \tag{11b}$$

Rearranging, we have

$$T(\omega)B_o(\omega) = \frac{s_{bb}(\omega)}{A_o(r_c,\omega)\, 2\pi r_c^2 \int_{\pi}^{\theta_o} B_F(\omega,r_c,\theta)\sin\theta d\theta}\,. \tag{12}$$

The quantity in the numerator is determined experimentally and factors in the denominator are computed.

3.4. Image Formation

Signal processing employed in the computer was identical for both experimental and theoretical images and consisted of linear amplification and peak detection. The pixel value anywhere in an image was defined to be the maximum value of the envelope of the amplified echo signal corresponding to the pixel of concern. Image files, consisting of 100 x 93 pixels and representing 2 cm x 1.86 cm regions in the phantom, were transferred to a Siemens CT image display system to produce hard copy. All images to be shown (both experimental and theoretical) were recorded using identical window level, window width and photography settings. Thus, an absolute quantitative comparison has been provided.

4. RESULTS

Theoretical and experimental images obtained with the 2.25 MHz and the 3.5 MHz transducers are displayed in figures 3 and 4, respectively. In both cases, the depth range of the imaged region is 8-10 cm. A mean pixel value, $\bar{x}$, computed for each image is also shown.

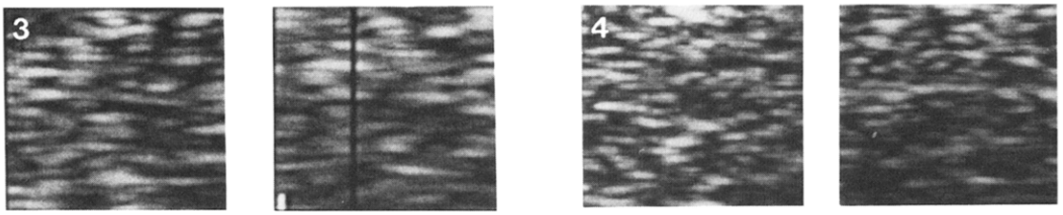

Fig. 3 Gray scale images from an 8-10 cm depth range in the phantom, produced with a 2.25 MHz transducer. x refers to mean pixel values for both the experimental (right) and model predicted (left) image.

Fig. 4 Gray scale image from an 8-10 cm depth range in the phantom, produced with a 3.5 MHz transducer. Results of the model (left) are compared with experiment.

To evaluate how well the model predicts signal levels and B-mode echo texture at different depths, theoretical images were also generated for ranges of 2-4 cm, 5-7 cm as well as 8-10 cm for the 3.5 MHz transducer. These are presented in figure 5 alongside images generated experimentally from the same depth ranges in the phantom. Mean pixel values again are shown.

Finally, examples of first and second order statistics computed from both the theoretical and experimental images are compared in figures 6 and 7, respectively. Both examples correspond to the images in figure 4. Each histogram in figure 6 includes all pixels in the corresponding image. The

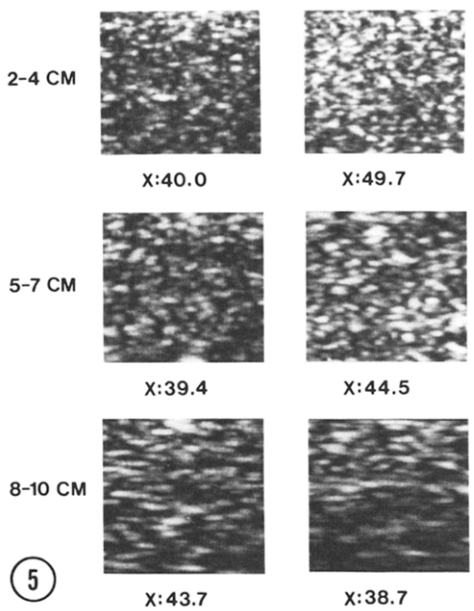

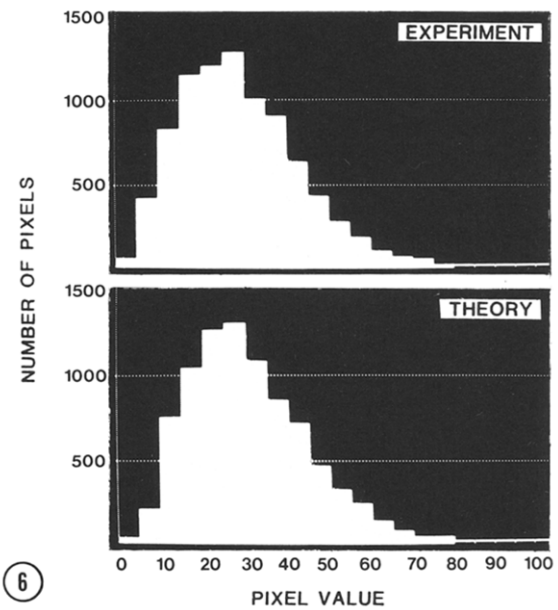

Fig. 5 Images generated with the three dimensional model (left) and corresponding to experimentally (right), 3 different depths in the phantom and the 3.5 MHz transducer. x refers to mean pixel values for each image.

Fig. 6 Pixel value histograms for the images in figure 4.

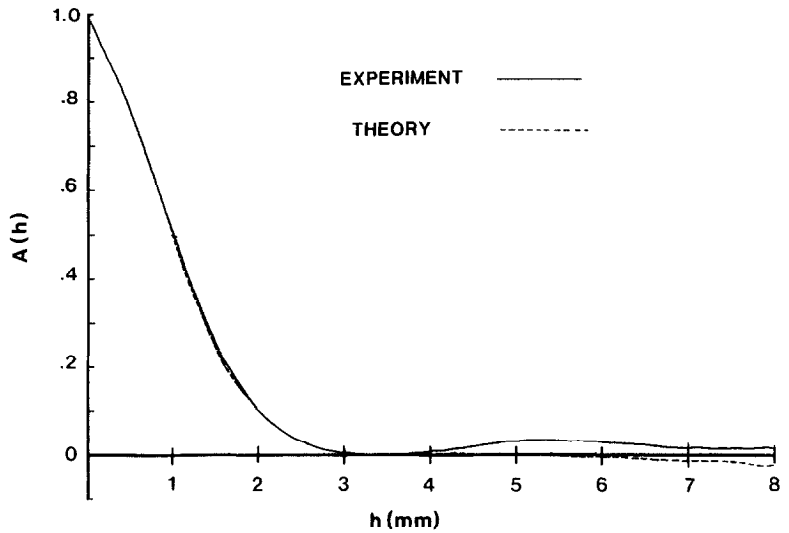

Fig. 7 Normalized autocorrelation function for images obtained with the 3.5 MHz, 19 mm diameter transducer and a depth range of 8-10 cm in the phantom.

normalized autocorrelation functions in figure 7 were computed using the method described by Foster et al. [5] and correspond only to lateral shifts, h, for the entire image in both cases. We express this autocorrelation function as

$$A(h) = \frac{\sum_{j=1}^{n_y} \sum_{i=1}^{n_x} [B(x_i - h, y_j) - \bar{B}]\,[B(x_i, y_j) - \bar{B}]}{\sum_{j} \sum_{i} B(x_i, y_j - \bar{B}]^2}, \tag{13}$$

where y_j refers to the axial coordinate of the (i,j) pixel and x_i refers to the lateral coordinate. $B(x_i, y_j)$ is the pixel value of the (i,j) pixel with a factor imposed to reverse approximately the effect of attenuation. This factor is

$$e^{2\alpha y_j},$$

where α is the attenuation coefficient of the TM material in the phantom at 3.5 MHz. Variations in α by as much as 20 percent had negligible effect on A(h). y_j is taken to be zero in the row of pixels closest to the scanning transducer. $\bar{B}$ is the mean pixel value, i.e.,

$$\bar{B} = \frac{1}{n_x n_y} \sum_{j=1}^{n_y} \sum_{i=1}^{n_x} B(x_i, y_j). \tag{14}$$

The values of n_x and n_y for this example are 100 and 93, respectively. Complete lack of correlation should result in a value of zero for the auto correlation function.

5. DISCUSSION

Visual (and, therefore, subjective) comparisons of corresponding pairs of theoretical and experimental images in figures 3-5 should convince the

reader that the pairs are quite comparable in texture qualities. Quantitative objective comparisons utilizing computed mean pixel values, pixel value histograms, and autocorrelation studies are likely more significant than visual comparisons. (The human eye-brain image analyzer is a highly sophisticated instrument, however, and should not be discounted [12].)

In figures 3-5, the ratios of the experimental mean pixel values to theoretical mean pixel values vary from a minimum of 40.0/49.7 = 0.80 for the 2 - 4 cm depth, 3.5 MHz case shown in figure 5 to a maximum of 43.0/38.7 = 1.11 for the 8 - 10 cm depth, 3.5 MHz case shown in figures 4 and 5. These ratios are shown to increase with increasing depth in figure 5; we are not certain why this variation was seen, but it might be related to uncertainties in the measurements of attenuation coefficients in the phantom material. On the other hand, the level of agreement between the model predictions and experimental results is very good: within 11 percent for the depth range between 5 and 10 cm and within 20 percent for that between 2 and 4 cm.

The histograms in figure 6 provide an elegant demonstration of the degree of quantitative agreement between the experimental and theoretical images. The histograms show the number of pixels for the various ranges of pixel values for the theoretical and experimental images of figure 4. The ratio of the mean to the standard deviation of these distributions is 1.99 (experiment) and 1.97 (theory), apparently in reasonable agreement with 1.91, the value predicted only on the basis of the Rayleigh probability distribution [13].

The normalized autocorrelation functions shown in figure 7 again show excellent agreement between theory and experiment. The solid line corresponds to experiment and the dashed line to theory. The two curves are almost identical through a value of h of about 4 mm.

The full width at half maximum amplitude (FWHM) of the autocorrelation function of image texture (for horizontal shifts) is related to the beam width of the ultrasound transducer.[13] For spherically focused transducers Wagner et al. [13] estimate that the FWHM is given by $0.8\ \lambda z/D$, where λ is the ultrasonic wavelength, z the axial distance and D the transducers projected aperture. For the results shown in figure 7 the FWHM is 2.1 mm; this agrees with a predicted value [13] of 2.15 mm if a frequency of 3 MHz is used to represent the ultrasound pulse from the transducer. This estimate cannot be applied gererally, however, without taking into account the broadband nature of such pulses, the frequency dependent scattering properties of the medium and effects of "beam hardening" caused by preferential attenuation of higher frequency components of a beam in tissue or a tissue-mimicking medium.

Sources of error in this study that might lead to discrepencies between theory and experiment should be mentioned:

a. Experimental uncertainties in the attenuation coefficients and the scattering properties in the tissue-mimicking phantom. We estimate our uncertainty in the attenuation coefficient slope as ±0.1 dB/cm. For low frequencies and short path lengths, this would not lead to significant errors. However, for higher frequencies and large depths, this can lead to substantial discrepencies between results predicted by the model and experimental results. For example, an uncertainty of 0.1 dB/cm leads to a 2 dB uncertainty in a 3 MHz echo signal component originating from a depth of 10 cm (about a 25 percent error).

b. Possible breakdown of the model at distances close to the transducer. The beam profile model may be inaccurate for points within about 2 cm of the transducer face [5,6]. Whether this could have a substantial effect on the present results isn't known, however. Also, any failure in the assumption that the glass bead scatterers behave as monopoles would lead to discrepancies between theory and experiment. Presumably, such discrepencies would be most severe at short transducer-to-imaged volume distances.

c. Experimental uncertainties introduced when recording echo signals from the phantom and from the reference reflector.

In spite of these sources of error, the overall agreement between predictions of the model and experimental results from the phantom is quite good. The results of this study demonstrate that the three-dimensional model performs adequately in predicting echo signals quantitatively and in predicting gray scale texture.

Two additional factors related to this study should be pointed out. The method for determining the complex function, $T(\omega)B_0(\omega)$, which depends on the transducer-pulser-receiver combination may have applications in clinical ultrasound. For example, if such calibration procedures were built into clinical instruments, it could lead to more satisfactory standardization of images than exists at the present time. For scanners which digitize echo signals prior to envelope detection, the $T(\omega)B_0(\omega)$ function could be calculated internally. This function is related to both the maximum sensitivity of the system and to the frequency bandpass characteristics. Secondly, the phantom described in this study is much more complete in its specifications than commercially available quality control phantoms. At the present time, it is difficult, if not impossible for clinical facilities to intercompare many phantom-based performance tests because of a lack of standardization of available phantoms. However, this study has demonstrated the feasibility of constructing tissue-mimicking phantoms which are not only well-characterized in terms of speed of sound and ultrasonic attenuation, but also in terms of scattering properties. If such phantoms were generally available, this could also aid in standardizing results among clinical facilities.

6. CONCLUSIONS

The present study demonstrates that a three-dimensional model for gray scale texture [1] can satisfactorily predict, absolutely and quantitatively, echo signal levels and image brightness when the ultrasonic attenuation and scatterer properties of an imaged volume are known. Passing such quantitative tests is additional evidence that the texture model is a reliable tool for computer simulations involving many important facets of ultasound B-mode imaging and tissue characterization.

The power of models such as the one described here lies in their potential use in simulation studies aimed at improving the diagnostic capabilities of clinical ultrasound instruments. Computer models could greatly facilitate investigations of factors such as tissue attenuation and scattering properties, transducer characteristics (frequency, bandwidth, aperture) as well as signal processing and image display parameters on the appearance and detectability of normal and abnormal structures in pulse-echo ultrasound images.

ACKNOWLEDGEMENTS

We are grateful to Kathy McSherry and Colleen Schutz for assistance in typing this manuscript, to Orlando Canto for preparing figures and to

Dr. Michael Insana for writing the computer programs for digitizing experimental signal waveforms. This work was supported in part by NIH grants RO1-CA39224 and RO1-CA25634.

REFERENCES

[1] Goodsitt, M.M., Madsen, E.L., and Zagzebski, J.A, A three dimensional model for generating the texture in B-scan ultrasound images, Ultrasonic Imaging 5, 253-279 (1983).

[2] Madsen, E.L., Insana, M.F., and Zagzebski, J.A., Method of data reduction for accurate determination of acoustic backscatter coefficients, J. Acoust. Soc. Am. 76, 913-923 (1984).

[3] Beyer, R.T. and Letcher, Physical Acoustics, Chap. 1, p. 14., (Academic Press, New York, 1969),

[4] Morse, P.M. and Ingard, K.U., Theoretical Acoustics, Chap. 8, p.426, (McGraw-Hill, New York, 1968)

[5] Madsen, E.L., Goodsitt, M.M., and Zagzebski, J.A., Continuous waves generated by focused radiators, J. Acoust. Soc. Am. 70, 1508-1517 (1981).

[6] Goodsitt, M.M., Madsen, E.L., and Zagzebski, J.A., Field patterns of pulsed, focused ultrasonic radiators in attenuating and nonattenuating media, J. Acoust. Soc. Am. 71, 318-329 (1982).

[7] Foster, D.R., Arditi, M., Foster, F.S., Patterson, M.S. and Hunt, J.W., Computer simulations of speckle in B-scan images, Ultrasonic Imaging 5, 308-330 (1983).

[8] Madsen, E.L., Zagzebski, R.A., Banjavic, R.A., and Jutila, R. Tissue-mimicking material for ultrasound phantoms, Med. Phys. 5, 391-394 (1978).

[9] Madsen, E.L., Ultrasonically Soft-tissue-mimicking Materials, in Medical Physics of CT and Ultrasound, G. Fullerton and J. Zagzebski, eds., American Association of Physicists in Medicine, Monograph 6, (American Institute of Physics, New York, (1980).

[10] The diameter distribution measurements were done by J. Campbell, then at University of Rochester, Rochester, NY.

[11] Faran, J.J., Sound scattering by solid cylinders and spheres, J. Acoust. Soc. Am. 23, 405-418 (1951).

[12] Julesz, B., Experiments in the visual perception of texture, Scientific American 78, 34-43 (1975).

[13] Wagner, R., Smith, S., Sandrik, J. and Lopez, H., Statistics of speckle in ultrasound B-scans, IEEE Transactions on Sonics and Ultrasonics 30, 156-163 (1983).